Journal of Sound and Vibration 330 (2011) 1265–1284

Contents lists available at ScienceDirect

Journal of Sound and Vibration

journal homepage: www.elsevier.com/locate/jsvi

Experimental identification of pedestrian-induced lateral forces on footbridges

E.T. Ingólfsson [a,*], C.T. Georgakis [a], F. Ricciardelli [b], J. Jönsson [a]

[a] Department of Civil Engineering, Technical University of Denmark, Building 118, Brovej, 2800 Kgs. Lyngby, Denmark
[b] DIMET, University of Reggio Calabria, Via Graziella - Feo di Vito, 89122 Reggio Calabria, Italy

ARTICLE INFO

Article history:
Received 15 February 2010
Received in revised form
21 September 2010
Accepted 30 September 2010
Handling Editor: J. Macdonald
Available online 10 November 2010

ABSTRACT

This paper presents a comprehensive experimental analysis of lateral forces generated by single pedestrians during continuous walking on a treadmill. Two different conditions are investigated; initially the treadmill is fixed and then it is laterally driven in a sinusoidal motion at varying combinations of frequencies (0.33–1.07 Hz) and amplitudes (4.5–48 mm). The experimental campaign involved 71 male and female human adults and covered approximately 55 km of walking distributed between 4954 individual tests. When walking on a laterally moving surface, motion-induced forces develop at the frequency of the movement and are herewith quantified through equivalent velocity and acceleration proportional coefficients. Their dependency on the vibration frequency and amplitude is presented, both in terms of mean values and probabilistically to illustrate the randomness associated with intra- and inter-subject variability. It is shown that the motion-induced portion of the pedestrian load (on average) inputs energy into the structure in the frequency range (normalised by the mean walking frequency) between approximately 0.6 and 1.2. Furthermore, it is shown that the load component in phase with the acceleration of the treadmill depends on the frequency of the movement, such that pedestrians (on average) subtract from the overall modal mass for low frequency motion and add to the overall modal mass at higher frequencies.

1. Introduction

The widely publicised closure of Paris' Solférino and London's Millennium footbridges in 1999 [1] and 2000 [2] have led to an understanding on the part of engineers and architects of the need to evaluate the potential for footbridge vibrations that can be attributed to pedestrians. Within the scientific community, the closures has also led to the initiation of a new tract of research, focused on the understanding of pedestrian loading, bridge response and their interaction. A plethora of research on the topic now exists [3–10] and as a consequence, numerous other bridges of different length and type have also been found prone to similar excessive lateral vibrations when exposed to large pedestrian crowds [11–15].

Only few national and international codes of practice and official design guidelines currently exist to help the designer address this issue. Most of these are based on the main hypotheses, that pedestrian-induced lateral loads can be modelled as velocity proportional loads or as "negative dampers", resulting from the "synchronised" lateral movement of pedestrians. This pedestrian lateral excitation mechanism is often characterised as synchronous lateral excitation (SLE) or

* Corresponding author. Tel.: +45 4525 1766; fax: +45 4588 3282.
E-mail address: eti@byg.dtu.dk (E.T. Ingólfsson).

0022-460X/$ - see front matter © 2010 Elsevier Ltd. All rights reserved.
doi:10.1016/j.jsv.2010.09.034

Nomenclature

a	parameter in a power law fit
A_j	fitting parameters in a spectral load model
b	parameter in a power law fit
B_j	fitting parameters in a spectral load model
c_p	velocity proportional pedestrian load coefficient
$\overline{c}_p$	mean value of the velocity proportional pedestrian load coefficient
$\hat{c}_p$	estimated error of the velocity proportional pedestrian load coefficient
Co_{Fx}	co-spectral density between F and x
DLF_j	dynamic load factor of load harmonic j
$\overline{\mathrm{DLF}}_j$	mean value of the dynamic load factor of load harmonic j
f	frequency
f_L	frequency of the lateral motion of the treadmill
f_n	natural frequency of a single-degree-of-freedom system
f_{Ny}	Nyquist frequency
f_p	pedestrian pacing frequency
f_w	pedestrian walking frequency
$\overline{f}_w$	mean pedestrian walking frequency
F	pedestrian-induced lateral force
$\hat{F}$	measurement error
F_D	damping force
$F_{D,\mathrm{eq}}$	equivalent pedestrian damping force
F_E	elastic restoring force (spring force)
F_i	lateral force peaks (i=1…3)
F_I	inertia force
$F_{I,\mathrm{eq}}$	equivalent pedestrian inertia force
G_j	amplitude of load harmonic j
H_n	frequency response function of a single-degree-of-freedom system
$\hat{k}$	calibration constant
K_n	stiffness of a single-degree-of-freedom system
m_p	pedestrian body mass
M	mass of stage 3 of the treadmill ergometer device
N_{av}	number of windows used to calculate a particular PSD
p	probability density function
$P_{D,\mathrm{eq}}$	average work done by $F_{D,\mathrm{eq}}$ per unit time
P_F	average work done by F per unit time
Qu_{Fx}	quad-spectral density between F and x
S_F	PSD of F
S_{Fj}	PSD of F around load harmonic j
$S_{F\,x}$	cross-spectral density between F and x
$S_{F\dot{x}}$	cross-spectral density between F and $\dot{x}$
t	time
T_{tot}	total signal duration
T_w	fundamental period of lateral pedestrian-induced load
v_p	pedestrian walking speed
W	body weight
x	lateral displacement of the treadmill
$\dot{x}$	lateral velocity of the treadmill
$\ddot{x}$	lateral acceleration of the treadmill
x_0	lateral displacement amplitude of the treadmill
$\dot{x}_0$	lateral velocity amplitude of the treadmill
$\ddot{x}_0$	lateral acceleration amplitude of the treadmill
δf	frequency resolution in a spectrum
Δf	bandwidth
ζ_n	damping ratio of a single-degree-of-freedom system
μ_X	sample mean of X
ξ	parameter in the lognormal distribution
ρ	linear correlation coefficient
ϱ_p	acceleration proportional pedestrian load coefficient
$\overline{\varrho}_p$	mean value of the acceleration proportional pedestrian load coefficient
$\hat{\varrho}_p$	estimated error of the acceleration proportional pedestrian load coefficient
σ_{DLF_j}	standard deviation of the DLF of load harmonic j
σ_F^2	total area of the PSD of F (total signal variance)
$\sigma_{\hat{F}}$	standard deviation of the error of the pedestrian-induced load
$\tilde{\sigma}_F^2$	area of the PSD of F in a specific frequency range
$\tilde{\sigma}_{F,j}^2$	area of the PSD of F around load harmonic j
$\sigma_{F\dot{x}}$	total area of the cross-spectral density between F and $\dot{x}$
$\tilde{\sigma}_{F\dot{x}}$	area of the cross-spectral density between F and $\dot{x}$ within a specific frequency range
$\tilde{\sigma}_{F\ddot{x}}$	area of the cross-spectral density between F and $\ddot{x}$ within a specific frequency range
$\tilde{\sigma}_{u,\mathrm{eq}}^2$	total area of the equivalent power spectral density of u
$\tilde{\sigma}_{u,j}^2$	area of the PSD of u around load harmonic j
$\hat{\sigma}_V$	standard deviation of the measured voltage signal from load cells
σ_X^2	sample variance of X
σ_x	standard deviation of x
$\sigma_{\ddot{x}}$	standard deviation of $\ddot{x}$
ϕ_j	phase angle of load harmonic j
ϕ_{xF}	phase spectrum between x and F
φ	phase angle
χ	parameter in the lognormal distribution
ω	angular frequency
ω_L	angular frequency of the treadmill motion
Cov[]	covariance operator
E[]	expected value operator
$\mathcal{F}$[]	Fourier transform operator
Re[]	real part operator
Var[]	variance operator

human–structure "lock-in" [2,11,16]. The UK National Annex to Eurocode (EN 1991-2) [17], the HIVOSS guidelines [18] and the *fib* (2005) recommendations [19] are for the most part based on this hypothesis. Alternatively, the French Road Agency (Sétra) has published a guideline in which the lateral acceleration, calculated assuming random pedestrian behaviour,

should be limited to 0.10 m/s^2. The value is chosen, so as to avoid SLE [20] and thus the destabilising effect of excessive negative damping. The limit is based on research carried out during the temporary closure of the Solférino Bridge. Results from a limited number of controlled pedestrian crowd tests indicated that there is a transition point at which a rapid increase in the lateral bridge response is triggered. The transition is explained as random pedestrian walking that becomes "synchronised" when lateral bridge accelerations increase beyond 0.10 m/s^2.

Although the current codes of practice and guidelines help to improve the designer's ability to predict the potential for large amplitude lateral footbridge vibrations, it should be recognised that they are based on a limited understanding of the actual phenomenon. This can be understood by examining the origins of the physical models they rely on. Those that utilise the concept of negative damping, employ an empirically derived velocity-proportional pedestrian damping constant c_p=300 N s/m, which represents an averaged value for each pedestrian, derived from back calculations of the measured modal response during specific controlled crowd tests on the Millennium Bridge [2]. The constant is assumed to remain unchanged, regardless of frequency of bridge motion. Furthermore, its determination is highly susceptible to experimentally obtained parameters, such as mode shape, modal mass and pedestrian distribution; rendering the universality of its application questionable. Similarly, the Sétra guidelines rely on a binary frequency-independent acceleration criterion, which suggests that the same probability of synchronisation is assigned to all pedestrians independent of the ratio between their walking frequency and the lateral vibration frequency of the bridge.

In recent years, various researchers have studied the mechanics of pedestrian-induced lateral forces on a laterally vibrating surface. Different hypotheses exist about the complex nature of the human–structure interaction and unlike current codes of practice and design guidelines which are primarily based on empirical full-scale observations, many of these hypotheses are supported by theoretical modelling of the interaction [21–25], which lack the proper experimental evidence to support their applicability.

In this paper, an in-depth examination of frequency-dependent lateral forces produced by a pedestrian are analysed and presented. An extensive experimental campaign was carried out, where the characteristics of the lateral forces from 71 volunteering pedestrians were measured during treadmill walking, both on a fixed surface and during lateral sinusoidal motion at different combinations of frequencies (0.33–1.07 Hz) and amplitudes (4.5–48 mm). Emphasis is placed on the treatment of both the motion-induced forces, defined as equivalent velocity and acceleration proportional coefficients, and those measured on a fixed surface. All of the data are presented in a probabilistic manner which illustrates the randomness associated with both intra- and inter-subject variability.

2. Mechanics of pedestrian-induced lateral forces

2.1. Laterally fixed surface

During walking, a person generates a ground reaction force, or simply GRF, through the acceleration (and deceleration) of the centre of mass of their body. In general, the GRF can be represented by a three-dimensional vector which varies in time and in space due to the forward movement of the person [8].

The lateral components of the GRF are small, compared to the vertical ones, and are generated through the balancing of the body [26]. The shape of a generalised lateral force time history is shown in Fig. 1. A single footstep is characterised by three lateral force peaks, F_1 to F_3, with values around 4–5 percent of the body weight [27]. However, several factors influence the shape of the walking force which is governed by large intra- and inter-subject variability. The intra-subject variability denotes differences in the GRF of the same pedestrian measured at two different time instances and depends on the type of footwear, walking speed and random variations in the gait, mood of the person, etc. [8,28]. The inter-subject variability refers to the variability between different people and depends on physiological parameters of the pedestrians, age, gender, race, etc. [29].

Due to the intra-subject variability, the time history of the walking force is a narrow-band random process, centred around the fundamental lateral loading frequency, f_w (defined as half the pacing frequency, f_p) and its higher harmonics.

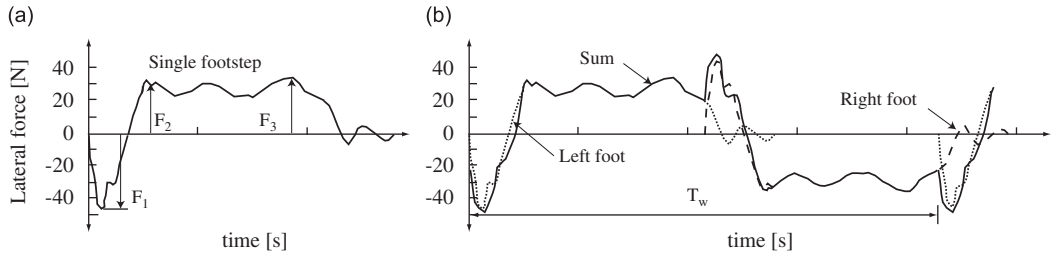

Fig. 1. Typical shape of a walking force from (a) a single footstep and (b) a series of consecutive footsteps (figure reproduced from [5]).

However, lateral walking forces are often modelled as a truncated Fourier series with a fundamental frequency, f_w, based on the simplified assumption that each footstep can be replicated from a single "characteristic" footstep (see Fig. 1):

$$F(t) = \sum_{j=1}^{n} G_j \sin(2\pi j f_w t - \phi_j) \tag{1}$$

where G_j and ϕ_j are the amplitude and phase angle of load harmonic j, respectively, and n is the number of load harmonics included in the truncated Fourier series. In most cases, the load amplitude is defined through the body weight normalised dynamic load factor $DLF_j = G_j/W$. According to Bachmann and Ammann [30], the values of the first five load harmonics are DLF_j={0.039; 0.01; 0.042; 0.012; 0.015}, j=1…5. In a later publication by same authors, the values of $DLF_1 = DLF_3 = 0.1$ are suggested for design purposes [31]. However, no justification for the difference is given. Other studies aimed at finding the DLFs from measured GRFs on stationary platforms indicate that they are independent of the walking speed and vary only slightly between males and females [32–34].

Non-zero load harmonics at even integer harmonics imply that the gait is asymmetric and that the walking is imperfect. This intra-subject variability was addressed by Pizzimenti [35], who used an instrumented treadmill to measure the continuous GRFs of 66 individuals. Ricciardelli and Pizzimenti [28] defined DLFs for an average (perfectly periodic) footprint as the sum of the contributions in the Fourier spectrum of the measured force in a narrow band around the frequency of the respective harmonic. The characteristic values (with 95 percent probability of non-exeedance) of the first five DLFs were reported as DLF_j = {0.04; 0.0077; 0.023; 0.0043; 0.011}, j=1…5. In the frequency domain, Pizzimenti and Ricciardelli [36] present a characteristic power spectral density (PSD), $S_{F,j}(f)$, for the first five load harmonics in a general (non-dimensional) form as

$$\frac{S_{F,j}(f)\cdot f}{\tilde{\sigma}_{F,j}^2} = \frac{2A_j}{\sqrt{2\pi}B_j}\exp\left\{-2\left[\frac{f/jf_w - 1}{B_j}\right]^2\right\} \tag{2}$$

where A_j and B_j are parameters determined by a data fit and $\tilde{\sigma}_{F,j}^2$ is the area of the PSD around the jth harmonic.

2.2. Lateral human–structure interaction

When walking on a laterally oscillating surface, it has been postulated that people tend to spread their legs apart and change their walking frequency and phase, to match that of the floor [16]. This alleged modification of the gait due to floor oscillations has become known within the civil engineering community as human–structure synchronisation. Early works by Fujino et al. [11] describe the concept of synchronisation. Their experimental studies on a human walking on a laterally moving platform showed that the walking frequency became synchronised to the platform frequency for lateral amplitudes in the range of 10–20 mm. This was used to explain the excessive lateral vibrations of the Toda Park Bridge in Japan during periods when the bridge is congested by large crowds. However, details regarding the platform tests have not been presented. Charles and Bui [37] defined the equivalent number of resonance pedestrians from back calculations of the measured response on the Solférino bridge and Danbon and Grillaud [38] used their result to propose a load model, where the number of synchronised resonance pedestrians increases linearly with the bridge displacement amplitude.

Strogatz et al. [21] offered a mathematical framework for the modelling of human–structure interaction, assuming that each pedestrian reacts to a weak stimulus from the bridge, either through the lateral displacement [21] or the acceleration [39]. If the stimulus is strong enough and the natural frequency of the bridge is close to the (original) walking frequency of the individual, the pedestrian locks into synchrony with the structure. The models are presented in the same framework as the theory of coupled oscillators, known from e.g. complex biological systems [40], but they lack any experimental evidence that can confirm their capability to predict pedestrian-induced lateral vibrations. According to Butz [33], only persons with natural walking frequency within 0.1 Hz of the lateral vibration frequency can synchronise with the structural motion. Similar observations were reported by Nakamura et al. [41], who investigated walking on the spot on a laterally moving shaking table. If the hypothesis that the correlated pedestrian force (or equivalent number of resonance pedestrians) increases with the vibration amplitude, due to an increasing number of synchronised pedestrians, is true, then the results by Butz [33] and Nakamura et al. [41] suggest that the susceptibility to SLE depends on the frequency ratio between the pedestrian walking frequency and the frequency of the lateral movement. This is contradictory to the basic assumption upon which current design recommendations are based.

An alternative approach is taken by Barker [42] who uses a simplified mechanical model of the human body centre of mass to show that synchronisation of the step is not a necessary precondition for diverging lateral vibrations to occur. Following along the same line, Macdonald [25] uses an inverted pendulum model to describe the lateral movement of the centre of mass and comes to similar conclusion. He argues that balance control is a matter of foot placement rather than timing of the step. His results are supported by full-scale measurements conducted on the Cliffton Suspension bridge during a period with large crowd-induced lateral vibrations [15].

2.3. Laterally moving surface

The importance of human–structure interaction when modelling pedestrian-induced lateral loading on long span footbridges has already been highlighted. Consequently, many researchers have attempted to measure pedestrian GRFs on

a laterally moving surface. Shortly after the closure of the London Millennium Bridge, platform tests were performed at Imperial College where it was found that the fundamental DLF increases with the lateral vibration amplitude and that at frequency 1.0 Hz there is a 40 percent probability of synchronisation or "lock-in", for vibration amplitudes of 5 mm [43]. However, very few details regarding these experiments have been published.

Similar platform tests were commissioned following the closure of the Solférino bridge in Paris [20], with the main conclusions being that the mean amplitude of the fundamental load harmonic is 35 N and that synchronisation with the platform does generally not occur for lateral accelerations lower than 0.15 m/s^2 [37]. Rönnquist [13] and Rönnquist and Strömmen [44] report that the lateral load increases both with an increase in the lateral acceleration of the structure and also as the walking frequency approaches the natural frequency of the platform. Similarly, Butz [33] reports that the DLF for a synchronised pedestrian depends of the structure and for the non-synchronised pedestrian the fundamental DLF should be taken as measured on a rigid surface. Common for all these tests however, is the fact that no distinction is made between pedestrian forces in phase with velocity or acceleration of the structure.

Phase synchronisation was initially addressed by McRobie et al. [16] who report that the load amplitudes can reach values as high as 300 N and the component in phase with the velocity of the structure can reach 100 N, when the vibration amplitude of the structure is 100 mm. Sun and Yuan [45] performed walking tests with seven individuals, using an instrumented treadmill fixed onto a shaking table. They concluded that for small vibration amplitudes, the relative phase between pedestrian and structure is variable (non-constant), but as the amplitude increases the phase becomes almost constant and the walking frequency changes to the vibration frequency. Furthermore, they find that on average the pedestrian load increases linearly with the acceleration and is 140.8° ahead of the bridge motion (S.D. 17.9°).

The experimental setup presented herewith (Treadmill Ergometer Device as described in Section 3) was initially constructed by Pizzimenti [35] and used in a pilot study with five different test subjects. The lateral GRFs were measured, and Pizzimenti and Ricciardelli [36] identified two different loading mechanisms; the first one centred around the walking frequency and its integer harmonics and the second one, *the self-excited force*, occurring at a frequency equal the vibration frequency. The self-excited force was further subdivided into in-phase and out-of-phase (with the displacement) lateral pedestrian load components. It is reported that the in-phase component of the force obtain negative values over the entire frequency range, which implies that pedestrians act as negative mass on the structure. This is in line with Macdonald's observations [25]. For the out-of-phase-component, pedestrians act as negative dampers, only for one combination of frequency and amplitude. At other frequencies, they add to the overall structural damping [36]. Since only five test subjects were used in the study and a limited number of frequencies and amplitudes were tested, the results can only serve as a qualitative indicator.

3. Current experimental investigations

3.1. Test subjects

During the summer of 2009, 71 healthy human volunteers (45 male and 26 female) with an age distribution according to Table 1, a mean height of 1.73 m (S.D. 0.01 m) and a mean weight of 74.4 kg (S.D. 15.1 kg) participated in an experimental campaign to determine pedestrian-induced lateral forces on a laterally vibrating platform. The lengths of the volunteers' legs were measured as well as the circumference of their wrist and ankle prior to the tests.

All tests which involved human test subjects were carried out in accordance with The Code of Ethics of the World Medical Association (Declaration of Helsinki) for experiments involving humans.

3.2. Experimental setup

A Treadmill Ergometer Device, positioned in the laboratory of the Inter University Research on Building Aerodynamics and Wind Engineering (CRIACIV) at the University of Florence in Prato, Italy, was used to measure the lateral GRF during walking, Fig. 2. The treadmill was built in 2003 at the University of Reggio Calabria [35] and moved to CRIACIV in 2006.

In brief, the treadmill consists of three separate parts, stages 1–3. The base of the treadmill, consisting of steel beams fixed on the laboratory floor is denoted by stage 1. Stage 2, which is a steel frame connected to the base through guide rails, such that it can move laterally, is driven by a motor. This motor controls the lateral vibration frequency of the system as well as the amplitude. Stage 3 consists of the walking surface with the dimension 100 × 180 cm, which is made of a steel frame system covered with plywood panels and a rubber belt. The belt is driven by a motor, which is attached to stage 2

Table 1
Age and gender distribution of test subjects.

	0–18 years	19–35 years	36–55 years	> 55 years	Total
Male	0	29	14	2	45
Female	1	16	9	0	26
Total	1	45	23	2	71

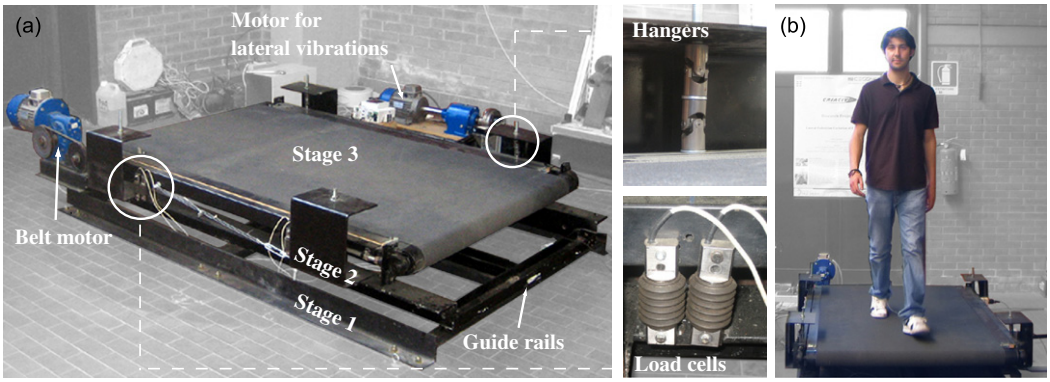

Fig. 2. (a) A treadmill ergometer device and (b) a pedestrian test subject during a walking test.

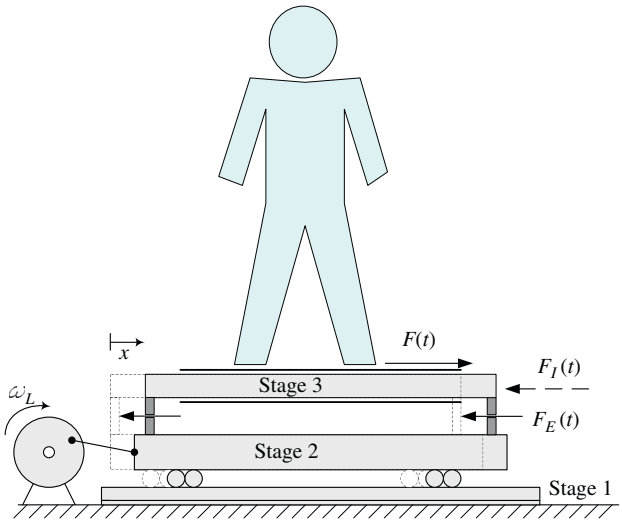

Fig. 3. A schematic overview of the treadmill ergometer device setup and the force equilibrium.

and therefore moves with the motion of the platform. The connection between stages 2 and 3, i.e. the belt and the laterally driven frame is twofold. First of all, it is vertically suspended from the supporting frame (at stage 2) using low friction hinges and secondly it is laterally supported with four flexural load cells. Images of various components of the treadmill are shown in Fig. 2. Both the motion of the belt and the lateral motion of the treadmill are driven by asynchronous 1.1 kW (1.5 HP) motors equipped with gearboxes. Both motors are controlled with inverters for variable belt speed and vibration frequencies, respectively. A schematic representation of the system is shown in Fig. 3. The experimental setup is a slightly modified version of that described by Pizzimenti and Ricciardelli [36] and Ricciardelli and Pizzimenti [28].

3.3. Other equipment

The resulting horizontal lateral force between stages 2 and 3 is measured with four load cells. Each load cell can measure up to 500 N with a sensitivity of 3.7711 mV/N. The motion of the treadmill is measured with two high sensitivity (10 V/g) ICP accelerometers (PCB Piezotronics, type 393B12). The accelerometers are connected to a 4 channel signal conditioner (PCB Piezotronics, type 441A42). Furthermore, the displacement of the treadmill is measured using a laser with sensitivity 100 mV/mm. The walking speed is determined using an encoder that measures the rotation of the steel cylinder which drives the treadmill belt. All signals were acquired with ± 5 V 24-Bit data acquisition modules (National Instruments, cDAQ-9172 and National Instruments, BNC 9234) at a sampling rate of 2048 Hz.

3.4. Test procedure

Subjects were requested to perform two types of walking on the treadmill; one without lateral motion of stage 3 of the treadmill (denoted static tests) and one with lateral sinusoidal movement at various vibration frequencies and amplitudes

Table 2
Test matrix which shows the number of different subjects tested at each particular combination of lateral vibration amplitude and frequency.

Frequency f_L/x_0 (Hz)	Lateral vibration amplitude						
	4.5 mm	10 mm	19.4 mm	28.7 mm	31.0 mm	38.3 mm	48.0 mm
0	Static test—71 subjects						
0.33	45	65	59	35	36	48	60
0.40	45	65	59	35	36	48	60
0.43	45	65	59	35	36	47	59
0.47	45	65	59	35	35	47	58
0.50	45	66	60	35	36	47	58
0.60	46	66	60	35	35	47	22
0.70	46	66	60	34	34	47	18
0.77	45	65	59	34	31	46	14
0.80	46	66	59	34	29	44	11
0.83	46	66	59	34	27	32	8
0.87	46	66	59	33	10	23	4
0.90	46	66	59	33	9	21	3
0.93	46	66	59	33	8	17	2
0.97	46	66	58	21	8	14	2
1.00	46	64	57	21	7	12	2
1.03	45	64	57	15	6	5	0
1.07	45	64	56	14	6	5	0

(denoted dynamic tests). Initially, each subject was asked to walk on the treadmill and select a comfortable walking speed. This walking speed was subsequently used in both the static and the dynamic tests. Only one static test with a duration of 2 min was performed, whereas each subject performed several dynamic tests of 30 s duration, with vibration frequencies in the range 0.33–1.07 Hz and displacement amplitudes between 4.5 and 48 mm. Typically, each test subject spent between 1 and 2 h in the laboratory, depending on their availability and thereby the number of dynamic tests performed. The order in which the dynamic tests were performed was determined by a combination of random and systematic selections. After a successful completion of the static test, the displacement amplitudes of the treadmill were selected randomly. The pedestrian was asked to walk continuously on the treadmill at each particular amplitude whilst the frequency was increased in steps, from the lowest frequency tested to the highest one. Each step lasted 30 s plus a transition time interval during which the frequency was changed. After sweeping through all the frequencies, a short break was taken during which time the amplitude was changed. Generally, each subject was tested at both low, intermediate and large amplitude vibrations. Most of the tests were recorded with a digital video camera and all comments from the test subjects relating to the tests were recorded. The test matrix is given in Table 2, where the number in each cell indicates the number of different subjects tested for that particular combination of frequency and amplitude.

A total of 71 static tests were performed and 4883 dynamic tests, covering the total walking distance of approximately 55 km.

3.5. Data post-processing

Initially, the DC components of all the measured signals were removed and subsequently the signals were re-sampled from the original 2048 to 32 Hz, by applying a digital anti-aliasing lowpass FIR filter. The new (re-sampled) data were further lowpass filtered with a cutoff frequency of 8 Hz for the static tests and 5 Hz for the dynamic tests. The spectral densities presented herewith are generally estimated from an averaged periodogram of the measured time series. The periodograms are obtained by dividing the original time series into a number of windows (possibly overlapping) and calculating the discrete Fourier transform in each of them. No general rules can be made regarding the preferred shape of the window (rectangular, raised cosine, etc.), its size or overlap percentage as it depends on the particular application as well as a trade-off choice between the accuracy of the estimate and the desired frequency resolution [46,47]. Therefore, different methods have been used depending on the particular application and in the following the frequency resolution, δf, number of averages, N_{av}, and the selected window function will be accounted for each time a new spectrum is presented.

By taking advantage of the fact that the pedestrian-induced load is near-periodic with fundamental frequency equal the (average) walking frequency, the most severe type of spectral leakage can be avoided by assuring that each window contains an integer number of vibration cycles. This is achieved by identifying the dominant frequency in the signal from the periodogram of the original time series, which has been zero padded to a much longer length (here 2048 s) for enhancing the frequency resolution. Having identified the dominant frequency, the original time series is truncated such that each window contains (as closely as possible) an integer number of vibration cycles. In the dynamic tests, the fundamental period is taken as that of the lateral treadmill motion, determined from the periodogram of the zero-padded

displacement signal. This ensures that the self-excited portion of the pedestrian-induced load is represented by an integer number of vibration periods.

3.6. Calibration of the treadmill

A dynamic calibration of the treadmill was performed prior to the pedestrian tests to verify the sensitivity of the force transducers and to determine the accuracy of the measurements. The treadmill is constructed such that a sinusoidal base motion with angular frequency ω_L and amplitude x_0 is generated at stage 2, and stage 3 can therefore be treated as a single-degree-of-freedom (SDOF) system subject to the base motion $x(t)$. The stiffness of this SDOF system is governed by the stiffness of the load cells, which for all practical purposes may be treated as rigid. The equilibrium of forces (see Fig. 3) is written according to d'Alambert's principle as [50]

$$F_I(t)+F_D(t)+F_E(t)=F(t) \tag{3}$$

where $F_I(t)$ is the inertia force, obtained as the mass M of stage 3 multiplied with the acceleration $\ddot{x}(t)$, $F_D(t)$ is the damping force which is considered negligible, $F_E(t)$ is the elastic force in the system, i.e. the measured force in the load cells and $F(t)$ is the external (pedestrian-induced) lateral load which acts on stage 3.

A calibration of the treadmill was made for all amplitudes and all frequencies in the range 0.27–1.17 Hz in step of 0.03 Hz and similar post-processing as described in Section 3.5 is adopted. The measured acceleration signal is used to calibrate the load cells. The calibration constant, $\hat{k}$, defined as the transformation of the voltage output from the load cells to force, is determined from the measured standard deviation of the acceleration and strain signals, respectively. For each combination of lateral frequency and amplitude a value for the calibration constant was obtained as

$$\hat{k}_i = M\frac{\sigma_{\ddot{x},i}}{\sigma_{Vi}} \tag{4}$$

where $\sigma_{\ddot{x},i}$ and σ_{Vi} are the measured standard deviations of the acceleration signal and the load cell signals, respectively. The load cells showed a linear behaviour with a linear correlation coefficient $\rho = 0.99997$.

3.7. Static pedestrian walking tests

In the following, the power spectral density (PSD) of the pedestrian lateral force is defined as either a continuous or a discrete single sided spectrum such that

$$\mathrm{Var}[F]=\sigma_F^2=\int_0^{f_{\mathrm{Ny}}} S_F(f)\,\mathrm{d}f \cong \sum_{k=1}^{N/2+1} S_F(f_k)\delta f \tag{5}$$

where $S_F(f)$ is the spectral ordinate at frequency f, f_{Ny} is the Nyquist frequency (half the sampling rate), δf is the frequency resolution of the spectrum and N is the number of samples in the discrete Fourier transform. An example of a typical measured force time history and the corresponding normalised square-root PSD is shown in Fig. 4. The intra-subject variability in the loading is illustrated by the varying load amplitude in the time history and quantified through the distribution of the energy around the main load harmonics.

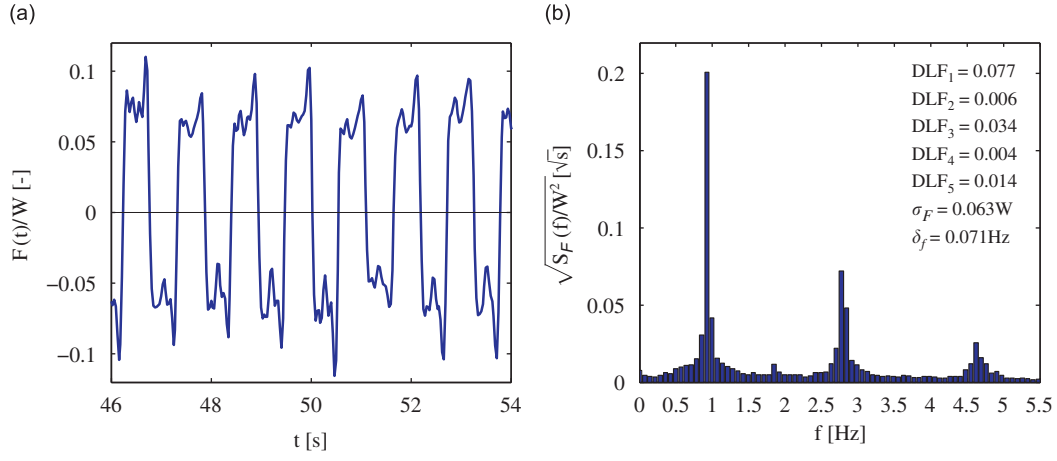

Fig. 4. Example of (a) a measured weight normalised force time-history and (b) the corresponding square-root PSD from a single pedestrian walking on a stationary surface (obtained with $\delta f = 1/15$ Hz and averaged over eight non-overlapping rectangular windows).

3.7.1. Equivalent "perfect" DLF

The intra-subject variability in the load makes a deterministic (and perfectly harmonic) description, similar to that in Eq. (1), only possible through an equivalent load amplitude [28,48]. The amplitude, or the equivalent perfect DLF, is obtained by requiring that the mean-square value of the response, $\tilde{\sigma}^2_{u,j}$, of a SDOF oscillator (with natural frequency, f_n), caused by the component of the measured force around load harmonic j, equals the mean-square response, $\tilde{\sigma}^2_{u,\mathrm{eq}}$, from a perfectly periodic force applied at resonance. The mean-square value of the response from the measured force is obtained as

$$\tilde{\sigma}^2_{u,j} = \int_{f_n - f_w/2}^{f_n + f_w/2} S_F(f)|H_n(f)|^2 \, \mathrm{d}f \tag{6}$$

$$|H_n(f)|^2 = \frac{1}{K_n^2}\left[\left[1-\left(\frac{f}{f_n}\right)^2\right]^2 + 4\zeta_n^2\left(\frac{f}{f_n}\right)^2\right]^{-1} \tag{7}$$

where $H_n(f)$, K_n, f_n and ζ_n are the frequency response function, stiffness, natural frequency and damping of the single-degree-of-freedom system, respectively, and f_w is the pedestrian walking frequency. The equivalent DLF can now be obtained from the following expression:

$$\tilde{\sigma}^2_{u,\mathrm{eq}} = \frac{1}{4K_n^2\zeta_n^2}\frac{\mathrm{DLF}_j^2 W^2}{2} = \tilde{\sigma}^2_{u,j} \tag{8}$$

The equivalent DLF depends on the modal damping and takes into account the filtering effect of the structure and that only load contributions in a narrow band near the natural frequency of the structure contribute to the vibration. As the modal damping ratio ζ_n and thereby the bandwidth may vary between structures, a conservative (upper-bound) value for the equivalent DLF is obtained by requiring that the mean-square value of the measured force, $\tilde{\sigma}^2_{F,j}$, in the total bandwidth between two harmonics ($\Delta f_j = f_w$) equals the mean-square value of the perfectly periodic force:

$$\tilde{\sigma}^2_{F,j}(\Delta f_j) = \int_{(j-1/2)f_w}^{(j+1/2)f_w} S_F(f) \, \mathrm{d}f = \frac{\mathrm{DLF}_j^2 W^2}{2} \tag{9}$$

Therefore, two different equivalent DLFs can be calculated; one according to Eq. (8), denoted the narrow-band model and one according to Eq. (9) denoted the broad-band model, i.e.

$$\mathrm{DLF}_j = \frac{2\sqrt{2}\zeta_n \tilde{\sigma}_{u,j} K_n}{W} \quad \text{narrow-band model} \tag{10}$$

$$\mathrm{DLF}_j = \frac{\sqrt{2}\tilde{\sigma}_{F,j}}{W} \quad \text{broad-band model} \tag{11}$$

The main problem with calculating the narrow-band DLF is that the accuracy of the spectral estimate decreases with a decrease in the bandwidth. This means that for low values of damping, the accuracy of the variance, $\tilde{\sigma}^2_{u,j}$, and thereby the equivalent DLF, relies on an accurate representation of the PSD in a very narrow band around the mean pacing rate. Due to the limited length of the measured force signal (2 min), the desired resolution to calculate the DLF for the narrow-band model is obtained through a combination of averaging, windowing and zero-padding of the data. Firstly, the data are divided into seven windows with 50 percent overlap and pre-multiplied with a Tukey window (a rectangular function with cosine side lobes of width $n_w/4$, where n_w is the number of data points in the window). In each window, the data was subsequently zero-padded to the total length of 16 times the original length (approximately 8 min). The smoothed (average) spectrum was then used to calculate the narrow-band DLFs and the zero-padding thereby works as a smoothening interpolation between the distinct frequencies in the spectrum of the original time series.

3.8. Dynamic pedestrian walking tests

As mentioned in Section 2.3, a pedestrian walking on a laterally driven surface will exert forces at the walking frequency and its integer harmonics, as well as at the frequency of the lateral oscillation. Following Ricciardelli and Pizzimenti [28], the latter force component will be referred to as "the self-excited force". An example of the measured pedestrian force and its PSD is shown in Fig. 5 for a lateral vibration amplitude of 19.4 mm at the frequency 1.06 Hz. The shape of the force time history is considerably different from that of the static tests (Fig. 4), due to the presence of the self-excited force component at the lateral vibration frequency. The two peaks in the PSD also provide clear evidence that the pedestrian walking frequency is not synchronised with that of the treadmill, which is an important observation as many mathematical models rely on that assumption. The potential for human–structure interaction is treated in more detail in Section 4.3.1. Firstly, the nature of the self-excited component of the force must be quantified, as not only the amplitude but also its phase (related to the treadmill motion) is of importance. This is done by dividing it into two terms, one in phase with the

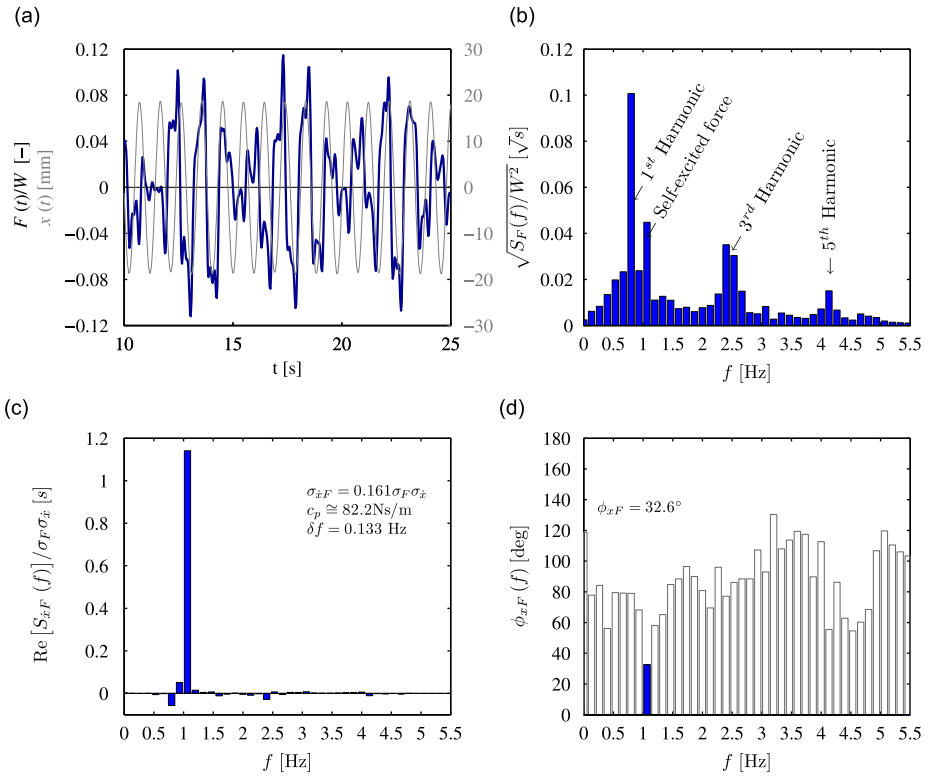

Fig. 5. Example of (a) a measured body-weight normalised force time-history, (b) its corresponding square-root PSD, (c) the normalised cross-spectral density between the measured lateral force and displacement and (d) the corresponding phase spectrum from a single pedestrian walking on a laterally oscillating surface (frequency 1.06 Hz and amplitude 19.4 mm). The spectra in (b)–(d) are obtained with $\delta f = 2/15$ Hz and averaged over four non-overlapping rectangular windows.

acceleration (inertial) and one in phase with the velocity (damping) of the treadmill, by considering the cross-covariance of the force and the treadmill motion.

3.8.1. Work done by pedestrian-induced lateral force

In a situation where a pedestrian is synchronised with the structure (or locked-in), the relative phase between the self-excited pedestrian force and the treadmill movement is constant and the phase angle can be determined. On the contrary, for a non-synchronised pedestrian, the phase angle may vary in time, whilst the pedestrian is still transferring energy into the structure. Therefore, the component in-phase with the velocity of the structure is determined through the average work done by the pedestrian per unit time P_F through integration of the product of the lateral pedestrian force $F(t)$ and the structural velocity $\dot{x}(t)$:

$$P_F = \frac{1}{T_{\text{tot}}} \int_0^{T_{\text{tot}}} F(t)\dot{x}(t)\,\mathrm{d}t \tag{12}$$

The integration in Eq. (12) is more conveniently evaluated in the frequency domain by considering the cross-covariance between the pedestrian force $F(t)$ and the platform velocity $\dot{x}(t)$ (at zero time lag). Recalling that the mean value has been removed from both $F(t)$ and $\dot{x}(t)$, the cross-covariance is written as [49]

$$\mathrm{Cov}[F,\dot{x}] = E[F(t)\cdot\dot{x}(t)] = \lim_{T\to\infty}\frac{1}{T}\int_0^T F(t)\dot{x}(t)\,\mathrm{d}t = \int_{-\infty}^{\infty} S_{F\dot{x}}(f)\,\mathrm{d}f \tag{13}$$

$$S_{F\dot{x}}(f) = \lim_{T\to\infty}\frac{1}{2\pi T}\mathcal{F}^*\{F(t)\}\mathcal{F}\{\dot{x}(t)\} = \mathrm{i}2\pi f\cdot S_{Fx}(f) \tag{14}$$

$$\Rightarrow S_{F\dot{x}}(f) = \mathrm{Co}_{F\dot{x}}(f) - \mathrm{iQu}_{F\dot{x}}(f) = \mathrm{i}2\pi f\cdot\mathrm{Co}_{Fx}(f) + 2\pi f\cdot\mathrm{Qu}_{Fx}(f) \tag{15}$$

$$\phi_{F\dot{x}}(f) = \arctan\frac{\mathrm{Co}_{Fx}(f)}{\mathrm{Qu}_{Fx}(f)} \tag{16}$$

where $\mathcal{F}\{\}$ is a Fourier transform operator, * denotes the complex conjugate and $i^2 = -1$. The cross-spectral density, $S_{F\dot{x}}(f)$, is complex and may be written in terms of its real part, denoted the co-spectral density $\mathrm{Co}_{F\dot{x}}(f)$, and the imaginary part called the quad-spectral density, $\mathrm{Qu}_{F\dot{x}}(f)$. Thereby, the cross-spectral density contains both the cross-amplitude and the phase between the processes $F(t)$ and $\dot{x}(t)$. It is further noted that for practical use of the cross-spectral density, all imaginary parts will cancel out, making only the real part of the spectrum of interest [49]. The last equality in Eq. (15) implies that the cross-spectral density between $F(t)$ and $\dot{x}(t)$ can be evaluated directly from the cross-spectral density between $F(t)$ and $x(t)$, simply by multiplying the spectrum with $i2\pi f$. This is convenient since the lateral treadmill displacement is measured directly, whereas the velocity can only be obtained through numerical differentiation of the measured displacement. The integral in Eq. (12) is now determined through integration of the cross-spectral density, either over the entire frequency domain, $P_F = \sigma_{F\dot{x}}$, or over a specific bandwidth, $\tilde{\sigma}_{F\dot{x}}(\Delta f)$. The latter approach is advantageous as it excludes erroneous contributions from correlated measurement noise or mechanical noise due to the possibility of non-perfect motion of the treadmill, which may occur at frequencies different from the fundamental lateral vibration frequency, see e.g. Fig. 5(c).The bandwidth is selected as $\Delta f = 0.05$ Hz centred at the lateral vibration frequency.

3.8.2. Damping and inertia proportional coefficients

It is now convenient to express the pedestrian force in terms of an equivalent damping force, $F_{D,\mathrm{eq}}(t)$, proportional to the velocity of the treadmill, and an equivalent inertia force, $F_{I,\mathrm{eq}}(t)$, proportional to its acceleration so that

$$F_{D,\mathrm{eq}}(t) = c_p\dot{x}(t) = c_p\dot{x}_0\sin(\omega_L t+\varphi) \tag{17}$$

$$F_{I,\mathrm{eq}}(t) = \varrho_p m_p\ddot{x}(t) = \varrho_p m_p\ddot{x}_0\sin(\omega_L t+\varphi+\pi/2) \tag{18}$$

where $\omega_L = 2\pi f_L$ is the angular frequency, $\dot{x}_0$ and $\ddot{x}_0$ are the velocity and acceleration amplitudes of the lateral vibration, φ is an arbitrary phase and m_p is the pedestrian mass. The average work done by the damping force per unit time is $P_{D,\mathrm{eq}} = \frac{1}{2}c_p\dot{x}_0^2$. The velocity proportional constant c_p is now obtained by imposing the condition that the pedestrian load inputs the same energy per unit time as that of the equivalent load within the frequency bandwidth Δf, thus $\tilde{\sigma}_{F\dot{x}}(\Delta f) = P_{D,\mathrm{eq}}$. The portion of the total pedestrian mass $\varrho_p m_p$ that contributes to the added mass of the structure is determined similarly to c_p, i.e.:

$$c_p = \frac{2}{\dot{x}_0^2}\tilde{\sigma}_{F\dot{x}}(\Delta f) \tag{19}$$

$$\varrho_p m_p = \frac{2}{\ddot{x}_0^2}\tilde{\sigma}_{F\ddot{x}}(\Delta f) \tag{20}$$

$$\tilde{\sigma}_{F\dot{x}}(\Delta f) = \int_{f_L-\Delta f/2}^{f_L+\Delta f/2}\mathrm{Re}[S_{F\dot{x}}(f)]\,\mathrm{d}f = -2\pi\int_{f_L-\Delta f/2}^{f_L+\Delta f/2} f\,\mathrm{Qu}_{F\dot{x}}(f)\,\mathrm{d}f \tag{21}$$

$$\tilde{\sigma}_{F\ddot{x}}(\Delta f) = \int_{f_L-\Delta f/2}^{f_L+\Delta f/2}\mathrm{Re}[S_{F\ddot{x}}(f)]\,\mathrm{d}f = -4\pi^2\int_{f_L-\Delta f/2}^{f_L+\Delta f/2} f^2\,\mathrm{Co}_{F\ddot{x}}(f)\,\mathrm{d}f \tag{22}$$

An example of the application of the spectral analysis for the determination of the force coefficient c_p and the phase angle between the lateral pedestrian force and the treadmill displacement is shown in Fig. 5. According to the definition of the coefficients c_p and ϱ_p, in Eqs. (17)–(18), the self-excited force appears positive on the right-hand side of the equation of motion, thus positive values of c_p and ϱ_p indicate a decrease in the modal damping and mass, respectively.

3.9. Error estimation

From Eq. (3) it is apparent that in the absence of damping and external load, the measured force and the inertial force of stage 3 should be equal in magnitude and opposite in direction. Having calibrated the load cell (see Section 3.6), an estimate of the error can be made by considering the residual force $\hat{F}(t)$, measured for an empty treadmill and defined as

$$\hat{F}(t) = F_I(t)+F_E(t) \tag{23}$$

At each combination of lateral vibration frequency and amplitude, the velocity and acceleration proportional coefficients were calculated according to Eqs. (19)–(20), as well as the total standard deviation of the force. In Fig. 6 the results from these calculations are shown, which indicate the level of error expected in the tests. For the velocity and acceleration proportional load coefficients, the mean errors are -1.0 N s/m (S.D. 4.7 N s/m) and 0.3 kg (S.D. 2.3 kg), whereas the mean error on the total force is 1.2 N (S.D. 0.2 N). For all practical purposes, these errors have been considered acceptable.

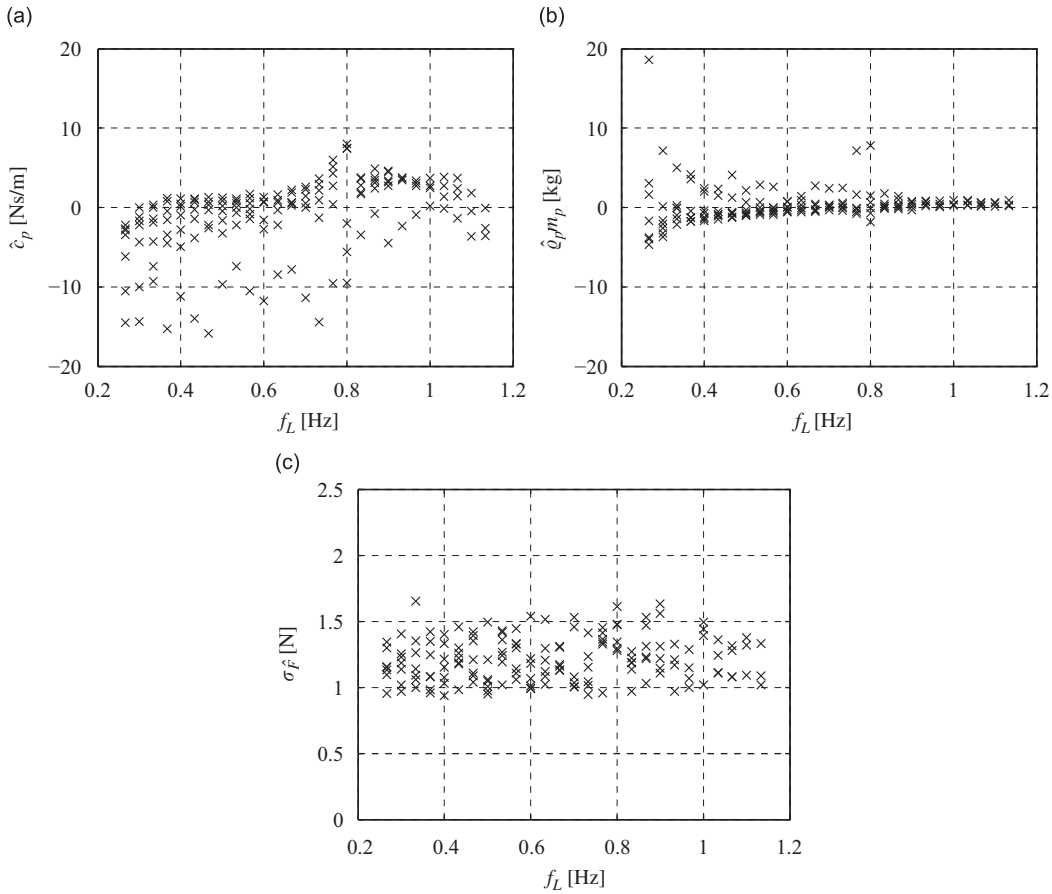

Fig. 6. Measured error for (a) velocity and (b) acceleration proportional load coefficients, respectively, and (c) standard deviation of error on total lateral force.

4. Results and discussion

4.1. Walking speed and frequency

The mean normal walking speed during the tests was 1.27 m/s (S.D. 0.23 m/s) for women and 1.30 m/s (S.D. 0.20 m/s) for men, while the mean normal walking frequency was 0.87 Hz (S.D. 0.09 Hz) for women and 0.85 Hz (S.D. 0.07 Hz) for men. The mean walking speed and walking frequency, $\overline{f}_w$, for all test subjects were 1.29 m/s (S.D. 0.21 m/s) and 0.86 Hz (S.D. 0.08 Hz), respectively, whereas the mean weight of the subjects was 730 N (S.D. 148 N), with a considerable difference between male (808 N and S.D. 110 N) and female subjects (603 N and S.D. 111 N). The probability distribution of the normal walking frequencies, as observed in the tests, can be approximated reasonably with a normal distribution, whereas the walking speed and the subject's weight are more randomly distributed.

A slight correlation between the walking speed and the walking frequency was observed (with linear correlation coefficient $\rho = 0.6612$). In Fig. 7 the pedestrian walking speed versus the walking frequency is shown, together with compiled data from earlier experiments conducted by Pansera [51], Terrier et al. [52] and Ingólfsson [53]. Ingólfsson et al. [54] used a power law of the type $f_w = a v_p^b$ to fit the experimental data (with $a = 0.81$ and $b = 0.35$) which is also shown in Fig. 7. Opposed to a linear regression, the advantage in using a power law is that it fulfills the boundary condition $v_p(0) = 0$, whilst allowing for non-constant values of the stride length.

Furthermore, a slight linear correlation was observed between the pedestrian weight and the RMS value of the pedestrian load ($\rho = 0.6720$). Their relationship is shown in Fig. 7, together with a linear regression, written as $\sigma_F = 0.041$ W. The other physical characteristics, such as length of leg or pedestrian height did not show signs of significant correlation with either the pedestrian force or the walking speed and frequency, confirming similar observations made by Ricciardelli and Pizzimenti [28].

4.2. Static pedestrian walking tests

Little to no correlation between the DLFs and the walking frequency could be observed from the tests. In Fig. 8 the DLFs of the first five load harmonics are shown as a function of frequency (normalised with the mean walking frequency of the

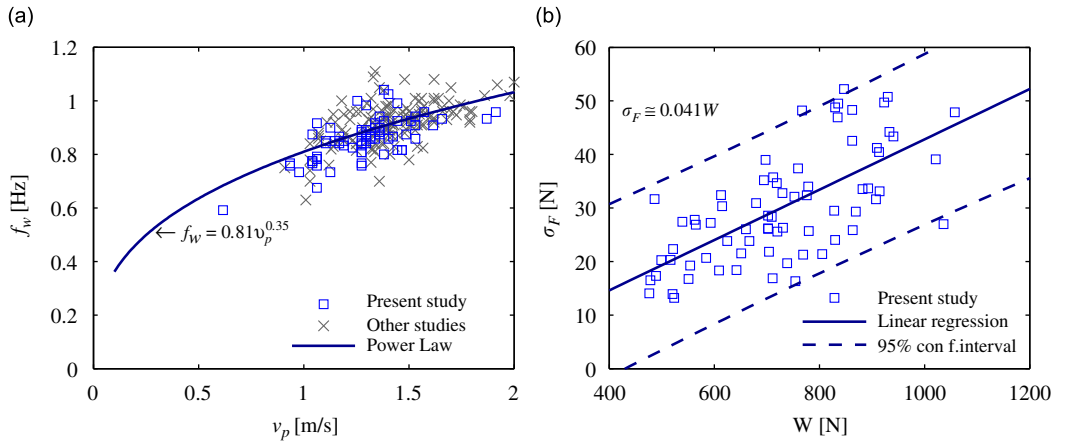

Fig. 7. (a) Relationship between the walking speed and the walking frequency measured in present study and as reported in other studies [54]. (b) Relationship between pedestrian weight and RMS value of the lateral pedestrian force.

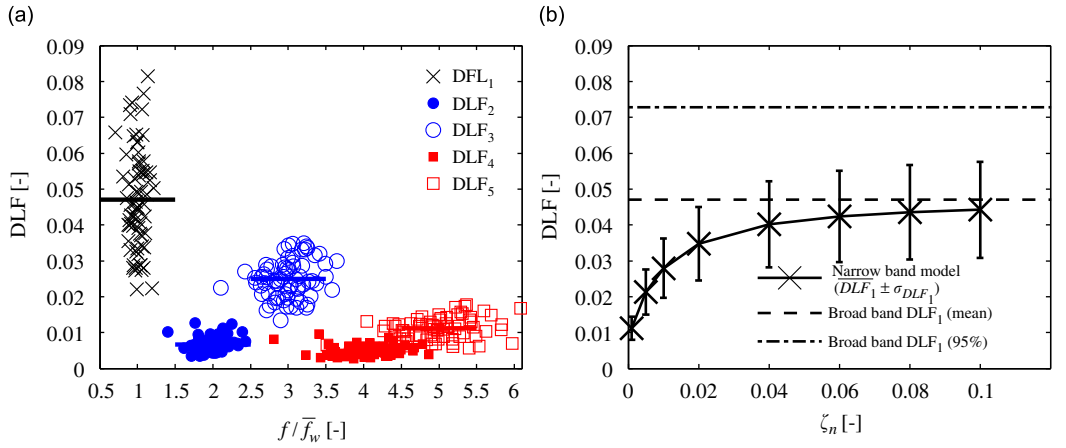

Fig. 8. Equivalent DLF obtained in the static tests using a broad-band model shown as (a) a function of the walking frequency and (b) a function of the damping ratio.

population, $\overline{f}_w$), calculated assuming a broad-band model as described in Section 3.7. Also, in Fig. 8, the fundamental DLF calculated using the narrow-band model is shown as a function of the damping ratio. It is noted that a considerable difference between the DLF calculated using the broad-band and the narrow-band models is observed, particularly at low structural damping ratios, as is characteristic for many long-span footbridges. This observation stresses the importance of intra-subject variability when calculating pedestrian-induced excitation and that the DLFs which are calculated on the basis of the broad-band model can be very conservative. Furthermore, the inter-subject variability in the DLFs is made clear by the large scatter of the measured data and an accurate description of the loading from a group of pedestrians seems only possible through probability distribution functions. The low mean value combined with large scatter suggests the use of a skewed distribution as a fit to the measured data, e.g. the lognormal distribution with the probability density function:

$$p(x) = \frac{1}{x\xi\sqrt{2\pi}} \exp\left[-\frac{[\ln x - \chi]^2}{2\xi^2}\right] \tag{24}$$

The parameters χ and ξ are related to the sample mean $E[X] = \mu_X$ and variance $\mathrm{Var}[X] = \sigma_X^2$ so that

$$\chi = \ln\mu_X - \frac{1}{2}\ln\left(1 + \frac{\sigma_X}{\mu_X^2}\right), \quad \xi^2 = \ln\left(1 + \frac{\sigma_X}{\mu_X^2}\right). \tag{25}$$

The experimentally obtained cumulative distribution functions of DLF_1, DLF_3 and DLF_5 (from the broad-band model) are shown in Fig. 9 together with the fitted lognormal distribution.

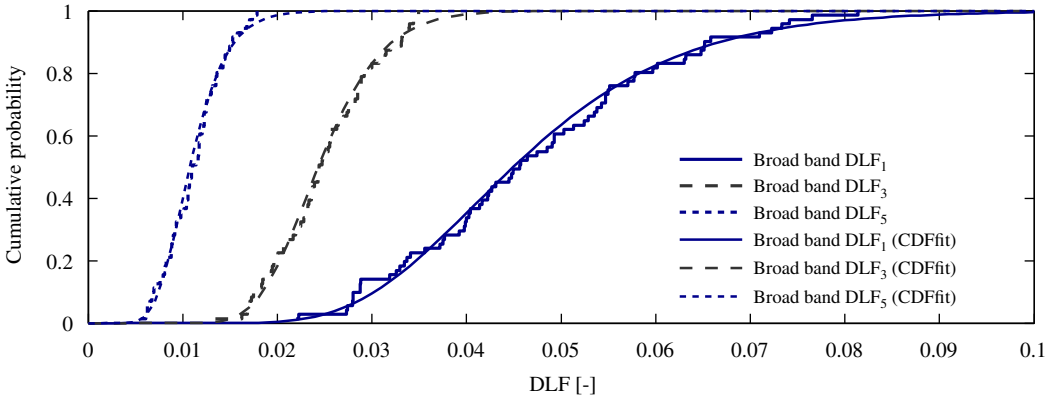

Fig. 9. Cumulative distribution function for the equivalent DLF of the odd harmonics using the broad-band model, shown with fitted log-normal distribution functions.

Table 3
Mean and characteristics values of the measured equivalent DLFs from the static pedestrian tests.

	j=1	j=2	j=3	j=4	j=5
Broad-band model, $\overline{\mathrm{DLF}}_j$ (mean value)	0.047	0.007	0.025	0.005	0.011
Broad-band model, DLF_j (95 percent fractile)	0.073	0.010	0.034	0.007	0.016
Narrow-band model ($\zeta_n = 0.01$), $\overline{\mathrm{DLF}}_j$ (mean value)	0.028	0.003	0.017	0.002	0.008
Narrow-band model ($\zeta_n = 0.01$), DLF_j (95 percent fractile)	0.041	0.006	0.024	0.002	0.012

The mean value of the DLFs and that with a 95 percent non-exceedance probability are shown in Table 3, both for the narrow-band (when assuming $\zeta_n = 0.01$) and the broad-band models. Clearly, there is a difference between these two methods, as illustrated in Fig. 8 and since the DLF depends on the structural damping, the most conservative method in a design situation is to use the broad-band model, in particular if the damping is uncertain or even unknown.

The results from the static tests compare generally well with the values reported by other researchers, see e.g. Section 2.1, both qualitatively in terms of data scatter and frequency dependency and also quantitatively in terms of characteristic values. In particular, the characteristic values of the DLFs reported by Ricciardelli and Pizzimenti [28] from the narrow-band model (with $\zeta_n = 0.01$) agree very well to those reported herewith, as expected since the experimental setups are (near) identical and the test subjects are drawn from a similar pool of persons. It is further shown that the lognormal distribution provides a reasonable fit to the data and may be used to model the probability distribution of the DLFs. This is especially useful when modelling the pedestrian-induced loading in a probabilistic sense e.g. through Monte Carlo simulations. It should be noted that these DLFs were measured in the absence of lateral vibrations and cannot be used for estimating vibrations in footbridges where the self-excited part of the load cannot be neglected.

4.3. Dynamic pedestrian walking tests

Pedestrian walking tests were performed at different lateral oscillation frequencies, f_L, and amplitudes, x_0, with up to 66 test subjects at each particular combination of f_L and x_0 (see Table 2). In each test, both the velocity and acceleration proportional constants c_p and ϱ_p were determined according to Eqs. (19) and (20), respectively. In Fig. 10, the mean value $\overline{c}_p$ for each lateral vibration frequency and amplitude is presented, both as a function of normalised frequency and amplitude. The frequency axis is normalised by the mean walking frequency of the population, $\overline{f}_w$.

In Fig. 10(a), the curves are made of an initial near-linear segment (up to $f_L/\overline{f}_w \cong 0.8$ on the horizontal axis), followed by an almost horizontal segment. The slope of the linear segment and the value of the constant segment increases with decreasing amplitude. At the lowest frequencies $\overline{c}_p$ is negative (i.e. damping is added to the structure), but at higher frequencies ($f_L/\overline{f}_w \gtrsim 0.50$) the coefficient is positive. In addition, in Fig. 10(b) there is a clear correlation between the mean load coefficient and the displacement amplitude at most frequencies. In particular for $f_L/\overline{f}_w > 0.89$, the negative damping decreases with increasing amplitude, which demonstrates the self-limiting nature of the associated structural response. At lower frequencies, the added damping decreases for an increase in the displacement amplitude.

The mean values of c_p presented herewith are lower than 300 N s/m as reported from the London Millennium Bridge [2]. It should be noted that a direct comparison between load coefficients c_p obtained in this study and that reported from the Millennium Bridge is not possible, first of all because on the Millennium Bridge the result is based on a limited number of full-scale experiments and may therefore represent a different fractile than the mean value. Secondly, the value of c_p

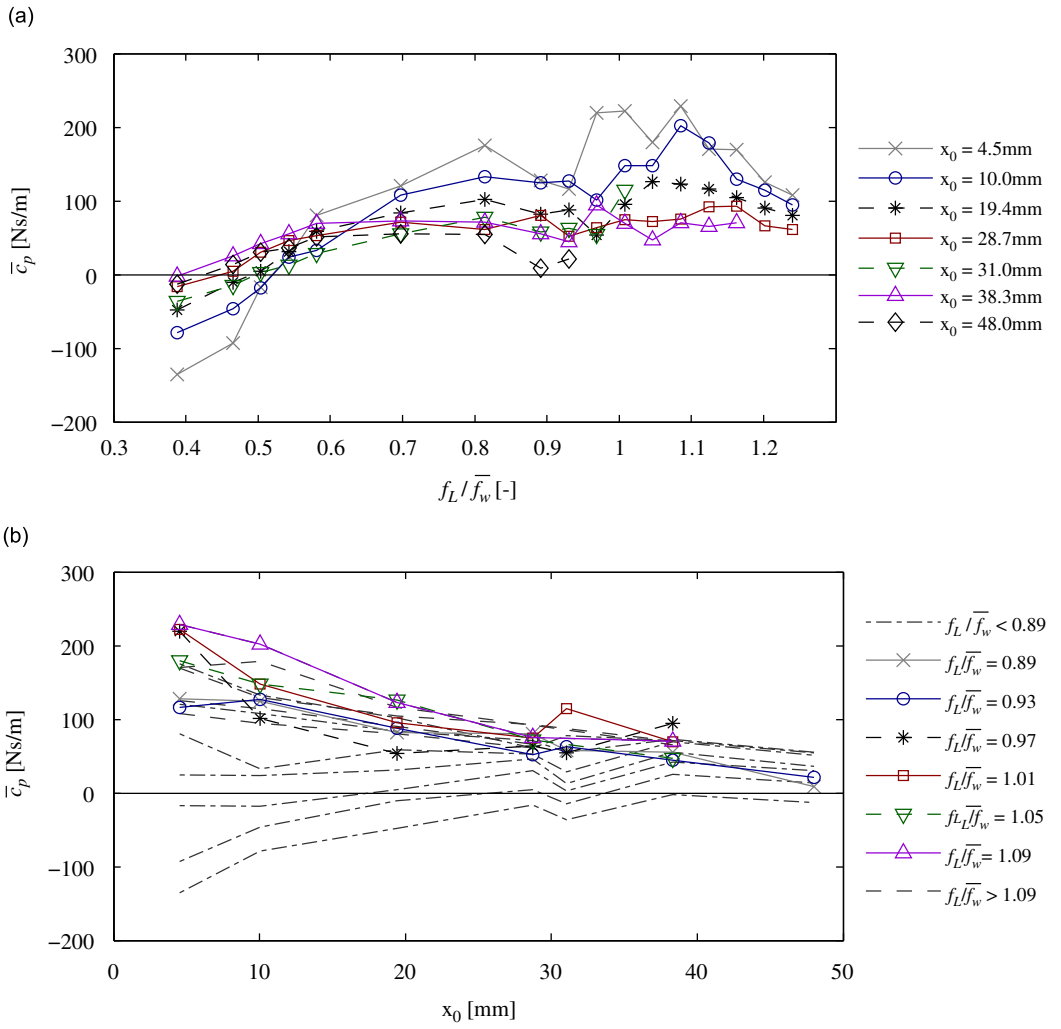

Fig. 10. Average value of the pedestrian load coefficient (a) as a function of the normalised frequency for different lateral displacement amplitudes and (b) as a function of the lateral displacement amplitude for various vibration frequencies.

reported by Dallard et al. [2] is estimated from back calculations of measured response and involves some inaccuracy in several bridge and crowd specific parameters; particularly modal mass, shape, damping and spatial pedestrian distribution. Based on the inverted pendulum model developed by Macdonald [15] the equivalent damping coefficient per pedestrian walking on a laterally moving surface was shown to depend strongly on the lateral oscillation frequency, with a maximum value of around 200 N s/m.

The mean value of the mass proportional constant, $\overline{\varrho}_p$, shows a clear dependency on the lateral vibration frequency. In Fig. 11(a) it is shown that at low frequencies, $\overline{\varrho}_p$ is positive and pedestrians therefore subtract from the overall modal mass of the structure. This effect of the pedestrian mass has been explained as "added stiffness" by Pizzimenti and Ricciardelli [36]. At higher frequencies however it becomes negative and near constant (at around 0.12–0.20), suggesting that pedestrians (on average) add to the modal mass of the structure. The transition from positive to negative values of $\overline{\varrho}_p$ occurs in the frequency range $f_L/\overline{f}_w \sim 0.55-0.85$ and is amplitude dependent, i.e. for large amplitudes, the transition frequency is generally lower. In Fig. 11(b), it is noted that at lower frequencies, $\overline{\varrho}_p$ decrease as the lateral vibration amplitude increases, but at higher frequencies it is near constant. The inverted pendulum model proposed by Macdonald [25] predicts positive values for ϱ_p (i.e. decreased modal mass) in the frequency range $f_L/\overline{f}_w \in [0.3; 1.3]$ and maximum value of 61 percent of the body weight. For lower frequencies, ϱ_p becomes negative with a maximum value of -1 at $f_L/\overline{f}_w = 0$. The results presented herewith contradict this, but as noted by Macdonald [25], the results from the inverted pendulum model depend on the specific control law used for the pedestrian balance control and with a different control scheme, positive values for ϱ_p are predicted in the low frequency range and negative values in the higher frequency range, similar to the results presented herewith.

Although the mean values show some clear frequency and amplitude dependency, it is stressed that a very large inter-subject variability was observed in the tests, illuminated by the large scatter in the measured load coefficients. Therefore,

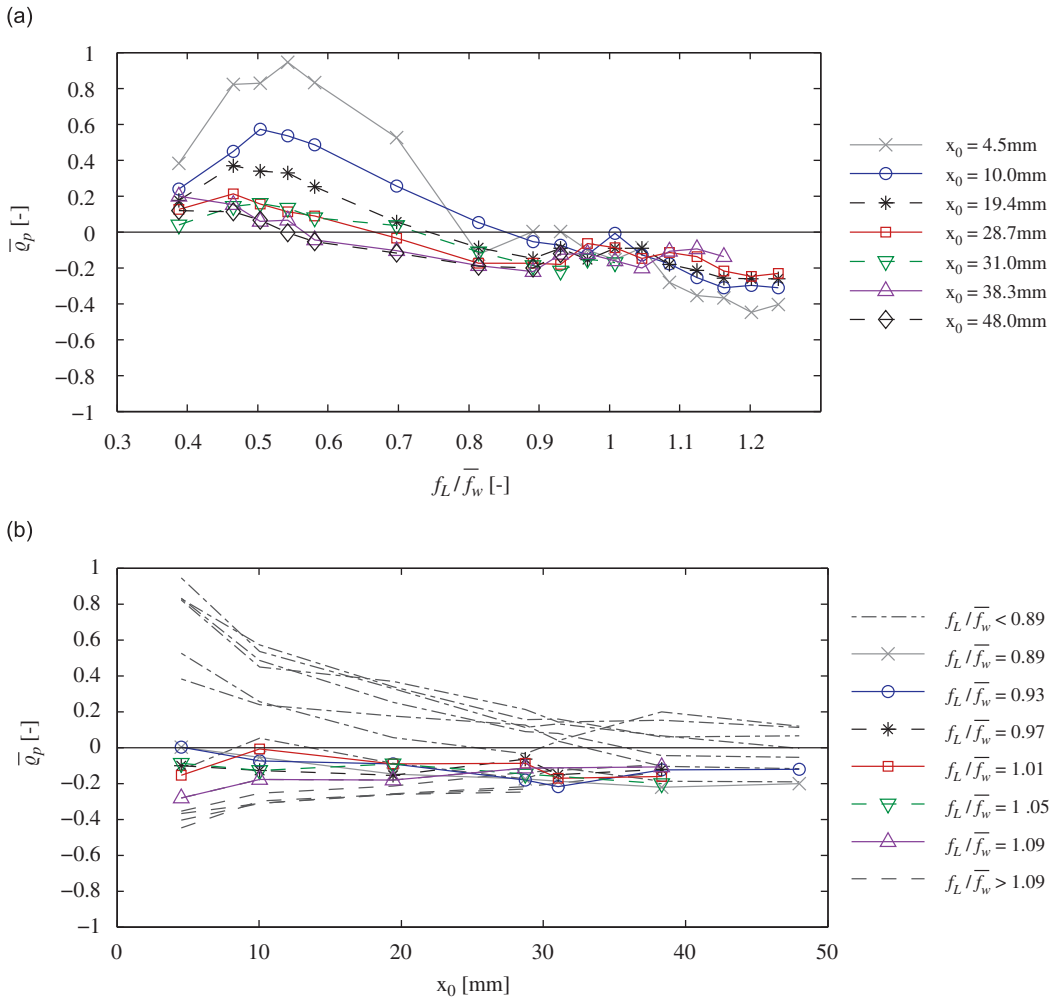

Fig. 11. Average value of the mass proportional coefficient $\overline{\varrho}_p$ (a) as a function of the normalised frequency for different lateral displacement amplitudes and (b) as a function of lateral displacement amplitude for various vibration frequencies.

the load coefficients are best described through their probability distribution and central moments (mean and standard deviation). In Fig. 12(a)–(b), the experimentally obtained probability distributions of c_p and ϱ_p for different frequencies are shown. In Fig. 12(c)–(d) the development of the mean value $\pm$one standard deviation error bar of the same load coefficients are shown as a function of the normalised lateral vibration frequency.

Further analysis reveals that the data scatter is particularly pronounced at low vibration amplitudes. The reason for this is found in the definition of the load coefficients in Eqs. (19) and (20), where it is noted that $\dot{x}_0^2$ and $\ddot{x}_0^2$ appear in the denominator and therefore causes a large magnification at low vibration amplitudes. This phenomenon is illustrated in Fig. 13, showing the mean value of the load and mass coefficients and the single standard deviation boundaries as a function of the lateral velocity and acceleration, respectively. We note that for c_p, the mean value is fairly constant over the entire amplitude range, but the standard deviation decreases as the velocity increases. The mass coefficient, ϱ_p, however, seems to decrease with the acceleration, with a positive value at low accelerations and a negative value in the acceleration range 0.1–0.4 m/s^2.

4.3.1. Qualitative assessment of the potential for human–structure synchronisation

From the tests various qualitative observations regarding the potential for human–structure synchronisation were made. In tests where the natural walking frequency coincided with the walking frequency of the test subject, people reacted differently; some would adjust their steps to match a "comfortable" phase, whilst others walked unaffected by the movement. Those who adjusted their phase to that of the treadmill, did so in different manner, i.e. some people spread the legs further apart whilst others crossed their legs during walking and therefore the load induced is different in these two situations. Furthermore, it was also observed that even the same person did not necessarily react in the same way in two nearly identical situations.

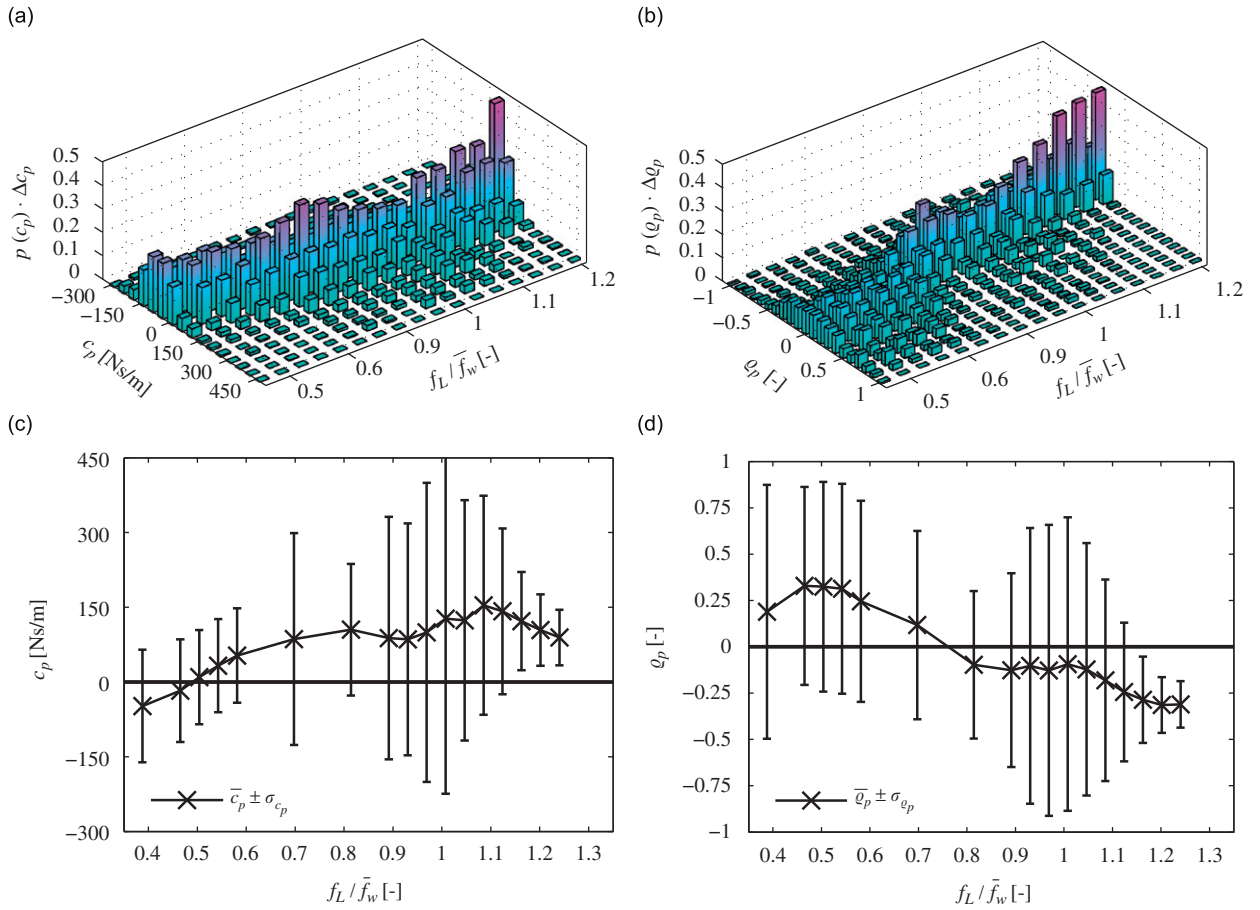

Fig. 12. Probability distributions of (a) damping proportional coefficient, c_p, and (b) inertia proportional coefficient, ϱ_p, at different frequencies shown as functions of the normalised frequency and mean value $\pm$ one standard deviation of (c) c_p and (d) ϱ_p.

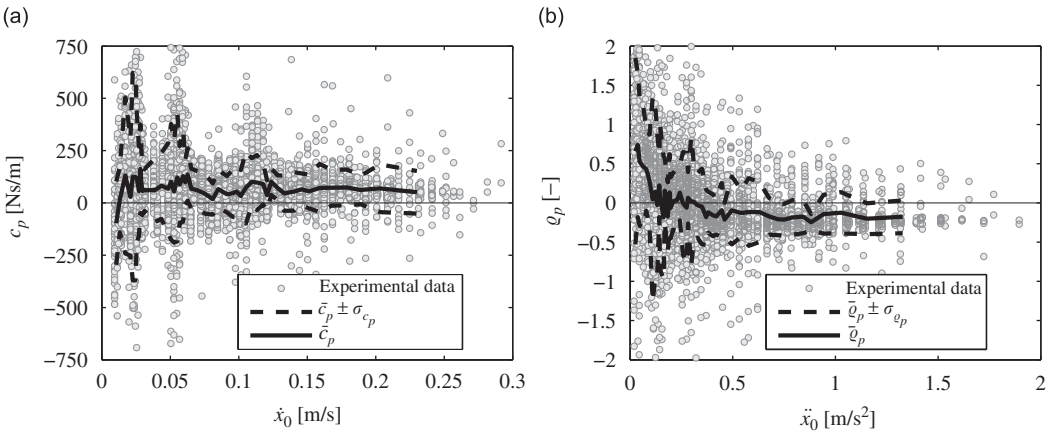

Fig. 13. Mean value $\pm$ one standard deviation of (a) c_p and (b) ϱ_p as functions of the lateral vibration velocity and acceleration, respectively.

Most of the test subjects felt at some point during the tests that they were affected by the lateral vibrations. The combination of low frequency and large amplitude was generally described as uncomfortable and several test subjects mentioned a resemblance to walking on a rocking boat. When the vibration frequency was close to the walking frequency, the vibration was often described as "clearly perceptible" or "annoying". The reason is that the relative phase between the treadmill movement and the steps changes slowly and thereby the reaction force from the treadmill (as felt by the

pedestrian) is constantly changing making it difficult to adapt to the vibration. This frequency range can be described as a potential "lock-in" range where people might tend to adjust their walking frequency to that of the treadmill lateral motion. In the tests presented herewith, this would be possible by adjustment of the stride length. However, a more efficient way would be to adjust the walking speed, which was not possible due to restrictions posed by the nature of the test equipment. Indeed, some of the test subjects made complaints that they would prefer to change their walking speed in an attempt to avoid the uncomfortable feeling of walking at a frequency close to the vibration frequency. Typically, these complaints would only occur during large amplitude vibrations, e.g. $x_0 \geq 19$ mm.

Additionally, it is worth pointing out that, although most of the pedestrians were affected by the lateral vibrations of the treadmill, the large scatter in the data and the visual observations made during the tests suggest that synchronisation of pedestrians walking on a laterally moving surface is neither generic nor obviously deterministic. Instead it is to a large extent governed by randomness and whilst some people feel comfortable adjusting to the platform motions, others are more comfortable walking at their own selected pacing rate. Whilst some people prefer adjusting their phase to match the displacement of the treadmill, others choose to match the acceleration or velocity.

The observed randomness in the behaviour of the pedestrians and lack of obvious signs of human–structure synchronisation, combined with the fact that negative damping could be generated at most frequencies, suggests that synchronisation is not as important as generally believed. To confirm this, further analysis were undertaken on the walking patterns of 7 test subjects that were instrumented with waist-mounted tri-axial accelerometers. These tests revealed that synchronisation is not a pre-condition for the development of velocity (and acceleration) proportional pedestrian forces, which may lead to large amplitude lateral vibrations in footbridges [55].

5. Conclusions

The data presented in this paper are based on measured forces from 71 pedestrians walking on both a laterally fixed and oscillating surface at various amplitudes and frequencies.

Particular attention is paid on quantification of the self-excited component of the pedestrian load through a damping proportional and a mass proportional coefficient, respectively. For both these coefficients, a large scatter is observed at low vibration amplitudes, but decreases as the amplitude increases. Analysis of the self-excited pedestrian load reveals that pedestrians (on average) consistently input energy into the structure in the normalised frequency range between approximately 0.6 and 1.2 and that the component in phase with the structural velocity can be modelled as a velocity proportional force. Interestingly, the coefficient of proportionality, c_p, decreases with an increase in the vibration amplitude and can therefore not be treated as a constant parameter (Fig. 10). Instead the load has a nonlinear component due to this dependency. The decrease in negative damping as the vibration amplitude increases, suggest that the pedestrian-induced loading is self-limiting. The component in phase with the acceleration is analysed and found to depend on the frequency of the structure. It is observed that for low frequencies, pedestrians subtract from the overall modal mass and add to the mass at higher frequency motion, with an amplitude-dependent transition.

The very large scatter in the data suggests that a probabilistic approach is necessary for an accurate estimation of the susceptibility of a footbridge to excessive vibrations. In particular, the critical number of pedestrian needed to trigger SLE may vary considerably depending on the particular crowd occupying the bridge.

Finally, since positive values of $\overline{c}_p$ occur in a broad frequency range, synchronisation of the walking frequency to that of the structure is not necessary for the development of velocity proportional loads, which can be represented in the form of negative damping.

Acknowledgements

The authors gratefully acknowledge Niccoló Bonanni, graduate student at University of Florence for his substantial contribution and enthusiasm in recruiting test persons for the experiments. Further, the authors also thank the people who participated in the tests presented in this study. A special gratitude is directed to the laboratory for Inter University Research on Building Aerodynamics and Wind Engineering (CRIACIV) at the University of Florence in Prato, Italy, who kindly hosted the experimental work, carried out during this research campaign, and in particular Lorenzo Procino chief engineer at CRIACIV is acknowledged for his help and support during this experimental work.

References

[1] P. Dziuba, G. Grillaud, O. Flamand, S. Sanquier, Y. Tétard, La passerelle solférino comportement dynamique (dynamic behaviour of the solférino bridge), *Bulletin Ouvrages Métalliques* 1 (2001) 34–57 (in French).
[2] P. Dallard, A. Fitzpatrick, A. Flint, S. Bourva, A. Low, R. Ridsdill-Smith, M. Willford, The London Millennium footbridge, *The Structural Engineer* 79 (22) (2001) 17–33.
[3] A. Pavic, P. Reynolds, Vibration serviceability of long-span concrete building floors. Part 1: review of background information, *The Shock and Vibration Digest* 34 (3) (2002) 191–211.
[4] A. Pavic, P. Reynolds, Vibration serviceability of long-span concrete building floors. Part 2: review of mathematical modelling approaches, *The Shock and Vibration Digest* 34 (4) (2002) 279–297.

[5] S. Živanović, A. Pavic, P. Reynolds, Vibration serviceability of footbridges under human-induced excitation: a literature review, *Journal of Sound and Vibration* 279 (1–2) (2005) 1–74.
[6] J. Brownjohn, S. Zivanovic, A. Pavic, Crowd dynamic loading on footbridges, *Proceedings of Footbridge 2008, Third International Conference*, Porto, 2008.
[7] M. Kasperski, Safety and serviceability of stand structures, *Proceedings of the 7th European Conference on Structural Dynamics*, Southampton, 2008.
[8] V. Racic, A. Pavic, J. Brownjohn, Experimental identification and analytical modelling of walking forces: literature review, *Journal of Sound and Vibration* 326 (2009) 1–49.
[9] F. Venuti, L. Bruno, Crowd-structure interaction in lively footbridges under synchronous lateral excitation: a literature review, *Physics of Life Reviews* 6 (2009) 176–206.
[10] A. Low, Design for dynamic effects in long span footbridges, *Proceedings of Footbridge 2008, Third International Conference*, Porto, 2008.
[11] Y. Fujino, B. Pacheco, S. Nakamura, P. Warnitchai, Synchronization of human walking observed during lateral vibration of a congested pedestrian bridge, *Earthquake Engineering & Structural Dynamics* 22 (9) (1993) 741–758.
[12] S. Nakamura, Model for lateral excitation of footbridges by synchronous walking, *Journal of Structural Engineering* 130 (1) (2004) 32–37.
[13] A. Rönnquist, Pedestrian Induced Vibrations of Slender Footbridges, PhD Thesis, Norwegian University of Science and Technology, 2005.
[14] Q. Ye, G. Fanjiang, B. Yanev, Investigation of the dynamic properties of the Brooklyn bridge, in: *Sensing Issues in Civil Structural Health Monitoring*, Springer, Netherlands2005, pp. 65–72.
[15] J. Macdonald, Pedestrian-induced vibrations of the Cliffton suspension bridge, UK, *Proceedings of the ICE: Bridge Engineering* 161 (BE2) (2008) 69–77.
[16] A. McRobie, G. Morgenthal, J. Lasenby, M. Ringer, Section model tests on human–structure lock-in, *Proceedings of the ICE: Bridge Engineering* 156 (BE2) (2003) 71–79.
[17] CEN, European Committee for Standardization, NA to BS EN 1991-2:2003 UK. National Annex to Eurocode 1: Actions on structure-Part 2: traffic loads on bridges, May 2008.
[18] C. Butz, C. Heinemeyer, A. Keil, M. Schlaich, A. Goldack, S. Trometer, M. Lukić, B. Chabrolin, A. Lemaire, P. Martin, A. Cunha, E. Caetano, Design of Footbridges-Guidelines and background document, HIVOSS, rFS2-CT-2007-00033, 2007.
[19] Fédération international du béton (*fib*), Guidelines for the design of footbridges, bulletin 32, November 2005.
[20] Sétra, Footbridges, Assessment of vibrational behaviour of footbridges under pedestrian loading, November 2006.
[21] S.H. Strogatz, D.M. Abrams, A. McRobie, B. Eckhardt, E. Ott, Crowd synchrony on the millennium bridge, *Nature* 438 (7064) (2005) 43–44.
[22] F. Venuti, L. Bruno, N. Bellomo, Crowd dynamics on a moving platform: mathematical modelling and application to lively footbridges, *Mathematical and Computer Modelling* 45 (2007) 252–269.
[23] J. Bodgi, S. Erlicher, P. Argoul, O. Flamand, F. Danbon, Crowd structure synchronization: coupling between Eulerian flow modeling and Kuramoto phase equation, *Proceedings of Footbridge 2008, Third International Conference*, Porto, 2008.
[24] G. Piccardo, F. Tubino, Parametric resonance of flexible footbridges under crowd-induced lateral excitation, *Journal of Sound and Vibration* 311 (2008) 353–371.
[25] J. Macdonald, Lateral excitation of bridges by balancing pedestrians, *Proceedings of the Royal Society A* 465 (2009) 1055–1073.
[26] F. Harper, W. Warlow, B. Clarke, The forces applied to the floor by the foot in walking. 1. Walking on a level surface, Technical Report, National Building Studies-Research paper 32, Department of Scientific and Industrial Research, 1961.
[27] E. Chao, R. Laughman, E. Schneider, R. Stauffer, Normative data of knee joint motion and ground reaction forces in adult level walking, *Journal of Biomechanics* 16 (2) (1983) 219–233.
[28] F. Ricciardelli, A. Pizzimenti, Lateral walking-induced forces on footbridges, *Journal of Bridge Engineering* 12 (6) (2007) 677–688.
[29] C. Sahnaci, M. Kasperski, Random loads induced by walking, *Proceedings of the 6th European Conference on Structural Dynamics*, Southampton, 2005.
[30] H. Bachmann, W. Ammann, *Vibrations in Structures. Induced by Man and Machine, Structural Engineering Documents, International Association for Bridge and Structural Engineering (IABSE)*, third ed., Zürich, Switzerland, 1987.
[31] H. Bachmann, A. Pretlov, H. Rainer, Appendix G: dynamic forces from rhythmical human body motions, *Vibration Problems in Structures: Practical Guidelines*, Birkhäuser, 1996.
[32] A. Crowe, M.M. Samson, M.J. Hoitsma, A.A. van Ginkel, The influence of walking speed on parameters of gait symmetry determined from ground reaction forces, *Human Movement Science* 15 (1996) 347–367.
[33] C. Butz, Beitrag zur Berechnung fußgängerinduzierter Brückenschwingungen (on the calculation of pedestrian-induced vibration of bridges), PhD Thesis, RWTH Aachen, 2006 (in German).
[34] C. Sahnaci, M. Kasperski, Excitation of buildings and pedestrian structures from walking and running, *Proceedings of Experimental Vibration Analysis for Civil Engineering Structures*, Porto, 2007, pp. 209–218.
[35] A. Pizzimenti, Analisi sperimentale dei meccanismi di eccitazione laterale delle passerelle ad opera dei pedoni (experimental analysis of the lateral pedestrian-induced mechanism of excitation of footbridges), PhD Thesis, Department of Civil and Environmental Engineering, University of Catania, 2003 (in Italian).
[36] A. Pizzimenti, F. Ricciardelli, Experimental evaluation of the dynamic lateral loading of footbridges by walking pedestrians, *Proceedings of the 6th International Conference on Structural Dynamics*, Paris, 2005.
[37] P. Charles, V. Bui, Transversal dynamic actions of pedestrians. synchronization, *Proceedings of Footbridge 2005, Second International Conference*, Venice, 2005.
[38] F. Danbon, G. Grillaud, Dynamic behaviour of a steel footbridge. Characterisation and modelling of the dynamic loading induced by a moving crowd on the Solferino footbridge in Paris, *Proceedings of Footbridge 2005, Second International Conference*, Venice, 2005.
[39] B. Eckhardt, E. Ott, S. Strogatz, D. Abrams, A. McRobie, Modeling walker synchronization on the millennium bridge, *Physical Review E* 75 (2007) 21110-1–21110-10 10.1103/PhysRevE.75.021110.
[40] S.H. Strogatz, From Kuramoto to Crawford: exploring the onset of synchronization in populations of coupled oscillators, *Physica D* 143 (1–4) (2000) 1–20.
[41] S. Nakamura, T. Kawasaki, H. Katsuura, K. Yokoyama, Experimental studies on lateral forces induced by pedestrians, *Journal of Constructional Steel Research* 64 (2008) 247–252.
[42] C. Barker, Some observations on the nature of the mechanism that drives the self-excited lateral response of footbridges, *Proceedings of Footbridge 2002, First International Conference*, Paris, 2002.
[43] M. Willford, Dynamic actions and reactions of pedestrians, *Proceedings of Footbridge 2002, First International Conference*, Paris, 2002.
[44] A. Rönnquist, E. Strømmen, Pedestrian induced lateral vibration of slender footbridges, *Proceedings of the 25th IMAC Conference*, Orlando, USA, 2007.
[45] L. Sun, X. Yuan, Study on pedestrian-induced vibration of footbridge, *Proceedings of Footbridge 2008, Third International Conference*, Porto, 2008.
[46] C. Chatfield, *The Analysis of Time Series. An Introduction*, sixth ed., Texts in Statistical Science, Chapman & Hall, CRC, 2004.
[47] D.E. Newland, *An Introduction to Random Vibrations, Spectral and Wavelet Analysis*, third ed., Longman Scientific & Technical, Essex, England, 1993.
[48] P.-E. Eriksson, Vibration of Low-frequency Floors—Dynamic Forces and Response Prediction, PhD Thesis, Chalmers University of Technology, Department of Structural Engineering, Göteborg, March 1994.
[49] E. Strömmen, *Theory of Bridge Aerodynamics*, Springer, 2006.
[50] R.W. Clough, J. Penzien, *Dynamics of Structures*, second ed., Civil Engineering Series, McGraw-Hill International Editions, 1993.
[51] A. Pansera, Analisi sperimentale delle caratteristiche del cammino ed azione dei pedoni sulle passerelle pedonali (experimental analysis of gait characteristics and walking-induced actions on footbridges), BSc Thesis, University of Reggio Calabria, 2006 (in Italian).
[52] P. Terrier, V. Turner, Y. Schutz, GPS analysis of human locomotion: further evidence for long-range correlations in stride-to-stride fluctuations of gait parameters, *Human Movement Science* 24 (1) (2005) 97–115.

[53] E. Ingólfsson, Pedestrian-induced Vibrations of Line-like Structures, MSc Thesis, Department of Civil Engineering, Technical University of Denmark, June 2006.
[54] E. Ingólfsson, C. Georgakis, J. Jönsson, F. Ricciardelli, Vertical footbridge vibrations: towards an improved and codifiable response evaluation, *Third international Conference on Structural Engineering, Mechanics and Computation*, Cape Town, South Africa, 2007.
[55] E. Ingólfsson, C. Georgakis, F. Ricciardelli, L. Procino, Lateral human-structure interaction on footbridges, *Tenth International Conference on Recent Advances in Structural Dynamics*, Southampton, 2010.